Hindawi
Structural Control and Health Monitoring
Volume 2024, Article ID 9945556, 20 pages
https://doi.org/10.1155/2024/9945556

Research Article

Comprehensive Assessment of the Seismic Performance of an Innovative Hybrid Semiactive and Passive State Control System for a Low-Degree-of-Freedom Structure Using Real-Time Hybrid Simulation

Bryan Castillo, Diego F. Ceron, Sharick M. Vides, Johannio Marulanda, and Peter Thomson

School of Civil and Geomatic Engineering, Universidad del Valle, Santiago de Cali, Colombia

Correspondence should be addressed to Bryan Castillo; bryan.castillo@correounivalle.edu.co

Received 20 October 2023; Revised 10 January 2024; Accepted 16 January 2024; Published 24 January 2024

Academic Editor: Chia-Ming Chang

The dynamic performance of base isolation systems provides an effective means to reduce the seismic vulnerability of buildings. However, large displacements in the base isolation during seismic events pose a major challenge for this control system. Recently, novel control systems have been implemented to control and reduce the excessive displacements. This study presents an evaluation of the seismic performance of unconnected-fiber-reinforced elastomeric isolators (U-FREI) and variable orifice damper (VOD) devices used together as a hybrid control system for a low-degree-of-freedom reference structure by employing real-time hybrid simulation (RTHS) testing technique. This physical cybernetic testing methodology allows a dynamic system of interest to be substructured into two components: numerical and experimental. In this study, the numerical substructure corresponds to a 2-degree of freedom model, representing a reference structure, and an experimental substructure was formed using the hybrid control system described. To develop an interface between the two substructures, a horizontal transfer system (HTS) was implemented and coupled with a vertical transfer system (VTS). Using RTHS, the performance of the reference structure and the hybrid control system was evaluated under six seismic events: CAM, CAT, El Centro, Loma Prieta, Pizarro, and Chihuahua, at a maximum acceleration of 0.10 g (0.981 $m{\cdot}s^{-2}$). The experimental behavior of the hybrid control system allows the reference structure to reduce its maximum drift by more than 24% compared to the fixed structure. Finally, the performance and accuracy of the RTHS tests were calculated.

1. Introduction

In recent years, structural engineering has focused on developing and implementing techniques to reduce seismic vulnerability in structural systems, while encouraging resilient designs that prioritize occupant safety [1–3]. Structural control systems have been extensively investigated and implemented in response to these performance requirements, improving the seismic response of civil structures using external devices [4], such as passive control systems [5–17], active control systems [18–22], semiactive control systems [23–27], and more commonly hybrid control systems [28–36]. Passive control devices have been the most widely adopted in buildings because of their lower installation and maintenance costs, lack of energy requirements, and low capacity to cause structural damage. In this sense, base isolator systems have become a reliable and cost-effective alternative for improving the seismic performance of civil structures [14, 16], creating a low-rigidity horizontal level between the structure and its foundation. This concentrates the deformation generated by seismic loads and reduces the energy induced in the structure, thereby reducing structural damage, repair costs, and the risk of loss of building functionality [4, 8]. Steel-reinforced multilayer elastomeric isolators (SREIs) are the most widely used base isolation devices. However, owing to

manufacturing techniques [37], the cost of importing [5], and the complexity of the required tests, there have been significant limitations for the widespread implementation of this technology in developing countries. Unconnected fiber-reinforced elastomeric isolators (U-FREIs) have been presented as an alternative to SREI device limitations, removing the mechanical connection to the structure and foundation and replacing steel-reinforcing plates with fiber laminates with similar mechanical characteristics [38], thereby reducing the weight and cost of the devices [39]. Pauletta et al. [40–42] conducted experimental tests to assess the dynamic behavior of U-FREI devices, while Spizzuoco et al. [43] and Madera et al. [5] conducted similar tests under controlled laboratory conditions. Losanno et al. [17, 44] implemented U-FREI technology as a base isolation system in a symmetrical 2-DOF steel-concrete structure, a methodology subsequently replicated by Riascos et al. [45]. Recently, Losanno et al. [46] and Calabrese et al. [47] employed U-FREI devices as base isolation systems aimed at reducing seismic vulnerability in unreinforced masonry (URM) buildings.

U-FREI devices, as a base isolation system, have limited seismic performance because of excessive lateral displacements, which require large areas of development to avoid damage to adjacent structures and generate additional costs to the technology [35, 36]. Viscous fluid damper (VFD) devices have been incorporated into several hybrid control systems to control excessive displacements in isolated buildings [30, 32–36, 48, 49], reducing the extensive protection zones. A notable feature of these control systems is the utilization of viscous dampers in the passive state [30, 33, 34] and magnetorheological dampers for semiactive systems [32, 35, 48, 49]. Variable orifice dampers (VODs) are a type of VFD that allow a wide range of controllability of the level of damping provided in civil structures, enabling a comprehensive range of hybrid control systems in passive or semiactive states [50]. Wongprasert and Symans [36] conducted an experimental evaluation of a semiactive hybrid control system for a 3-DOF steel building using an elastomeric base isolator system and VFD devices, which have traditionally been used as semiactive control devices in civil structures [30]. In this context, a systematic comparison between the passive and semiactive states of a hybrid control system composed of U-FREI devices as the base isolation system and VOD devices, as was carried out in this study, has not been reported in the literature.

The evaluation of hybrid control systems composed of base isolation and VFD has been primarily conducted on large-scale structures [51–53], which have limited their experimental assessment under real seismic performance conditions because of the lack of required equipment and excessive costs associated with constructing the test prototype. Therefore, the evaluation of this type of control system tends to be conducted numerically. In this sense, studies conducted by Dey et al. [32] and Losanno et al. [16, 17, 44] on low-degree-of-freedom structures permit resource optimization, structural response simplification, and a detailed experimental assessment of the seismic performance of the structural control devices used. In recent years, an innovative experimental testing methodology known as real-time hybrid simulation (RTHS) has been implemented to evaluate the dynamic performance of complete structural systems [54]. This approach was derived from methodologies employed in aerospace engineering testing [55] and was initially introduced in the field of structural engineering as an online test or hybrid simulation (HS). The methodology involves an experimental assessment of dynamic systems characterized by extended time scales, comprising a physical component devoid of inertial effects in continuous interaction with an analytical component [56, 57], which generates a communication interface through transfer systems, typically implementing hydraulic actuators and sensors. In the RTHS, the substructuring concept proposed in the HS is adapted to real-time timescales. This entails testing the most critical or interesting segment of the system, which typically exhibits nonlinear behavior when incorporating inertial effects [58, 59]. This testing methodology is particularly suitable for the evaluation of highly nonlinear devices such as base isolation systems or viscous fluid dampers. Experimental evaluations of base isolation systems as experimental substructures were performed by Lanese et al. [60] and Nakata et al. [61]. Recently, Riascos et al. [45] performed an RTHS test with U-FREI devices, taking the upper structure as a numerical substructure. Furthermore, viscous fluid dampers as experimental substructures have been extensively studied using RTHS [62–67]. Nevertheless, the behavior of VOD in passive and semiactive states has not been assessed to date using this innovative testing technique.

The versatility, potential, and acceptable accuracy of RTHS enable the concentration of resources on the evaluation of the specific components of interest within a system, which leads to reduced experimental setup costs, increased execution times, and the alleviation of capacity constraints often encountered in large-scale traditional dynamic experiments [68]. Therefore, in this study, the seismic performance of an innovative hybrid passive and semiactive state control system composed of U-FREI and VOD devices was evaluated for the low-degree-of-freedom structure proposed by Magliulo et al. [69] using an RTHS. This structure has become a reference structure when studying control systems, but it should be noted that a U-FREI-VOD hybrid control system has never been tested on this structure. The remainder of this paper is organized as follows. Section 2 provides details of the assessed reference structure and a description of U-FREI and VOD devices. In Section 3, the dynamic substructuring of the reference structure with a hybrid control system, transfer systems employed, experimental setup, and seismic excitations are described. Section 4 provides a detailed analysis of the seismic performance of the U-FREI and VOD used as a hybrid control system for the reference structure. In addition, it assesses the performance of the RTHS. Finally, Section 5 presents the conclusions of the study.

2. Main Structure

2.1. Reference Structure. The reference structure used, shown in Figure 1, was built at the University of Naples Federico II, Italy, with the objective of performing several seismic shake table tests on this structure to evaluate the seismic performance of base isolation systems [16, 17, 44, 45, 69–71]. This prototype had a scale factor of 1 : 3 for a total height of 2900 mm and a plan area (X-Y) of 2150×2650 mm. The structural system used was a heat-formed square hollow section steel, with dimensions of $120 \times 120 \times 12.5$ mm, and columns-welded hollow section steel with dimensions of $150 \times 150 \times 15$ mm. The upper-level beams were bolted to the columns, whereas the lower-level was considered a rigid node. Concrete blocks were added at both levels to provide a realistic weight to the structure. The structure has a mass of $m_1 = 3571$ kg at the lower level and a mass of $m_2 = 4155$ kg at the upper level. The dynamic properties of the structure when it is fixed to the ground were taken from the results obtained in [69], which describe a stiffness $K_f = 2.369 \cdot 10^6$ N·m^{-1}, a damping coefficient $C_f = 1.984 \cdot 10^3$ N·s·m^{-1}, and a damping ratio $\zeta = 1.0\%$. The fundamental frequency of the fixed structure in the x-direction is $f_f = 3.810$ Hz.

This reference structure has been used as an experimental test prototype and has been extensively detailed in the literature in recent years for the evaluation of structural control devices. Losanno et al. [17, 44] assessed the seismic behavior of U-FREI devices when subjected to bidirectional excitation, while the reference structure was supported by them, and concluded that these devices have significant potential in terms of reduction of the seismic vulnerability of the structure and cost-effectiveness of production using low-cost materials. Riascos et al. [45] conducted an RTHS using a numerical model of this structure with the aim of verifying the importance of considering the rocking effect in the behavior of U-FREI devices and concluded that considering this effect represents an increase in the isolator and structure displacement; however, it represents a reduction in the fundamental frequency of the structure and a significant increase in the isolation capacity. Calabrese et al. [70] performed a comparison between the results obtained in a shake table test and the results of an RTHS test, concluding that the RTHS is highly effective in validating the behavior of U-FREI devices supporting these types of structures. Magliulo et al. [69] conducted several shake table tests on this structure to obtain its dynamic properties. Subsequently, they tested the influence of gypsum board walls installed between the columns of the structure and concluded that these types of partitions do not contribute to the structural stiffness nor structural period; however, the study showed an increase in terms of damping, which has a beneficial effect on earthquake response.

2.2. Hybrid Structural Control System. The hybrid structural control system used in this study is composed of four U-FREI devices and two VOD devices, as shown in Figure 1. Each U-FREI device consists of 15.0 layers of rubber fiber, which are 2.0 mm thick; these layers were reinforced by 14.0 layers of 1.0 mm thick polyester fibers. The isolators had a total height of 44.0 mm and a diameter of 80.0 mm. Recently, Riascos et al. [45] conducted the RTHS tests mentioned in Section 2.1, using the same isolators. In addition, the parameters of the Bouc–Wen model that describe these devices numerically are calculated. These parameters were adopted in this study for the RTHS tests due to the testing framework for base isolators that have a capacity of only two specimens. The Bouc–Wen model is used to calculate the performance of 2 or 4 U-FREI devices, depending on the RTHS architecture. These architectures are explained later in this paper. The design, manufacturing, and validation processes of U-FREI devices can be found in [5]. In contrast, VOD devices are double-rod dampers with an external cylinder with a 210 mm stroke and an internal diameter of 25.40 mm. The rod had a diameter of 12.70 mm on each side of the piston and a total length of 700.0 mm. This damper is integrated with a needle valve that controls the flow of oil, which allows the specification of the nonlinear damping force. In addition, this device is equipped with a relief valve system that protects the seals and gate stem from excessive high pressures, which could damage the device components.

The damper has two operating modes: passive and semiactive. In passive mode, the valve opening level was selected and remained constant throughout the test. However, in semiactive mode, the valve opening changes based on the optimum force conditions required to reduce the base displacements, focusing on LQG (linear-quadratic-Gaussian) control [72]. The LQG controller implemented, shown in Figure 2, is fed with the measured displacement $u_{1,m}(t)$ and this controller calculates the optimal total force $F_{D\_\mathrm{opt}}(t)$ that the two VOD devices should provide to the structure to minimize drifts. This force is divided by two in order to calculate the optimal force $F_{\mathrm{opt}}(t)$ that each VOD has to supply, and the absolute value of the force is calculated as $|F_{\mathrm{opt}}(t)|$. The force error $e_f(t)$ compares in real-time $|F_{\mathrm{opt}}(t)|$ and the absolute value of the measured force $|F_{D,m}(t)|$ and feeds jointly with the measured force $F_{D,m}(t)$ the controller law that calculates the motor signal $u_{\mathrm{motor}}(t)$ which rotates the motor that controls valve's closure. The motor controller law evaluates the force the VOD applies to be between the limits allowed. Finally, $F_{D,m}(t)$ is multiplied by 2 to obtain the total force produced by both VOD devices $F_D(t)$, and this force feeds back the LQG controller and closes the loop. The device features a rotation servo motor with dimensions of $54 \times 44 \times 20$ mm and a minimum torque of 550 N-mm, designed to control the opening of the valve. This servo motor was installed on top of the valve using a 32-hole coupling piece that allowed position control. An optocoupler encoder FC-03 was utilized to control the rotation of the servo motor. The electromechanical operation was controlled using a microprocessor.

3. Real-Time Hybrid Simulation (RTHS)

3.1. Numerical Substructure (NS). The steel frame described in Section 2.1 was considered as the numerical substructure (NS), which does not include the hybrid control system. The behavior in the x-direction was analyzed using an analytical

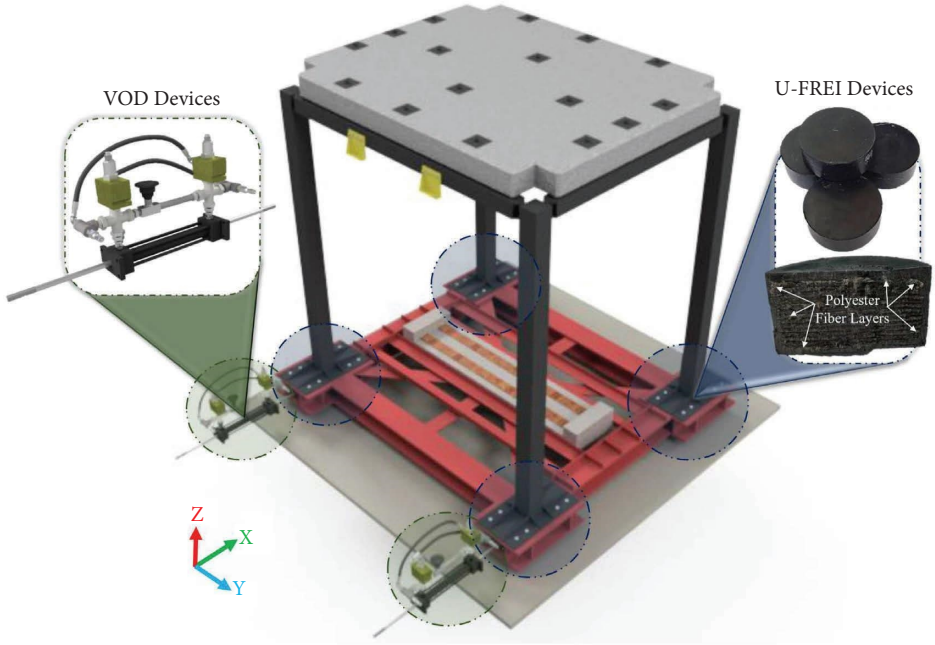

Figure 1: Scheme of the reference structure with a hybrid control system.

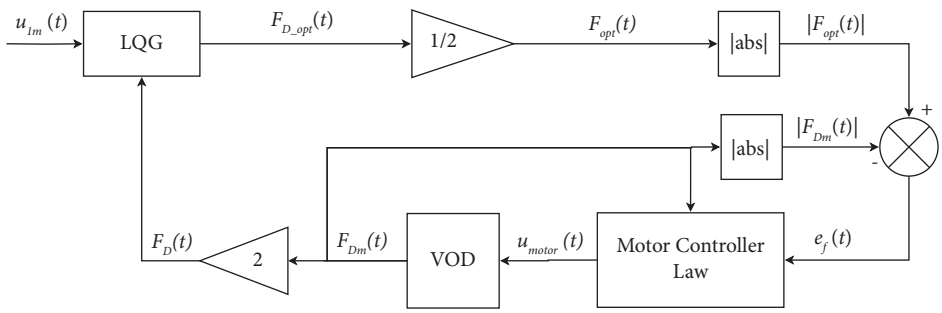

Figure 2: Scheme of the LQG control.

2-DOF model. The dynamic performance of this structure is described by equation (1), where M_r, C_r, and K_r are the mass, damping, and stiffness matrices, respectively, and $\ddot{x}$, $\dot{x}$, and x are the relative acceleration, velocity, and displacement vectors, respectively. The dynamic substructuring of the system allowed the extraction of the properties of the hybrid control system, as shown in equation (2), where the current matrices M_n, C_n, and K_n represent only the reference structure. The term $\Gamma_{\text{feed}} \cdot F_{\text{feed}}$ represents the restoring force of the experimental specimens (VOD and U-FREI devices), with the influence vector $\Gamma_{\text{feed}} = [1\,0]^T$ that indicates the DOF where this load was applied. Finally, $\ddot{a}_g$ represents the ground acceleration and the influence vector $\Gamma_g = [1\,1]^T$ indicates the DOF it influences. The complete system is expressed as a state-space model according to equations (3) and (4), which define a dynamic multiple-input multiple-output (MIMO) system with three inputs ($\ddot{a}_g$ and F_{feed} of the VOD and U-FREI devices) and 2.0 outputs U, corresponding to the displacements in each DOF.

$$M_r \cdot \{\ddot{x}\} + C_r \cdot \{\dot{x}\} + K_r \cdot \{x\} = M_r \cdot \Gamma_g \cdot \ddot{a}_g, \tag{1}$$

$$M_n \cdot \{\ddot{x}\} + C_n \cdot \{\dot{x}\} + K_n \cdot \{x\} = -M_n \cdot \Gamma_g \cdot \ddot{a}_g - \Gamma_{\text{feed}} \cdot F_{\text{feed}_{\text{UFREI}}} - \Gamma_{\text{feed}} \cdot F_{\text{feed}_{\text{VOD}}}, \tag{2}$$

$$\begin{Bmatrix} \dot{x} \\ \ddot{x} \end{Bmatrix}_{[4x1]} = \begin{bmatrix} 0 & I \\ -M_n^{-1}K_n & -M_n^{-1}C_n \end{bmatrix}_{[4x4]} \begin{Bmatrix} x \\ \dot{x} \end{Bmatrix}_{[4x1]} + \begin{bmatrix} 0 & 0 & 0 \\ -\Gamma_g & -M_n^{-1}\Gamma_{\text{feed}} & -M_n^{-1}\Gamma_{\text{feed}} \end{bmatrix}_{[4x3]} \begin{Bmatrix} \ddot{a}_g \\ F_{\text{feed}_{\text{UFREI}}} \\ F_{\text{feed}_{\text{VOD}}} \end{Bmatrix}_{[3x1]}, \tag{3}$$

$$\{U\}_{[2x1]} = \begin{bmatrix} I & 0 \end{bmatrix}_{[2x4]} \cdot \begin{Bmatrix} x \\ \dot{x} \end{Bmatrix}_{[4x1]} + \begin{bmatrix} 0 & 0 & 0 \end{bmatrix}_{[2x3]} \cdot \begin{Bmatrix} \ddot{a}_g \\ F_{\text{feed}_{\text{UFREI}}} \\ F_{\text{feed}_{\text{VOD}}} \end{Bmatrix}_{[3x1]}. \tag{4}$$

The extended Bouc–Wen model, as reported by Manzoori et al. in [73], was used to numerically model the dynamic behavior of the U-FREI devices. This model is given by the following equation:

$$F_{\text{Ia}}(t) = f_k(t) + f_d(t), \tag{5}$$

where $F_{\text{Ia}}(t)$ denotes the total shear force generated by the deformation of a single isolator, $f_k(t)$ denotes the hysteretic spring force, and $f_d(t)$ denotes the damping force. These forces were calculated using equations (6) and (7), respectively. Where the pseudo-displacement z is calculated using (8). The procedure for calculating the constants shown in Table 1, which are required for this model, and their specific explain of these parameters are described in [45].

$$f_k(t) = a_1 \cdot u_1 + a_3 \cdot {u_1}^3 + a_5 \cdot {u_1}^5, \tag{6}$$

$$f_d(t) = c \cdot \dot{u}_1 + b\left(1 - \frac{\beta}{A}|z|^n\right)z, \tag{7}$$

$$Y\dot{z}(t) = A\dot{u}_1 - \beta\dot{u}_1|z|^n - \gamma|\dot{u}_1|z|z|^{n-1}. \tag{8}$$

3.2. Experimental Substructure (ES). The experimental substructure (ES) was composed of the hybrid control system presented in Section 2.2. In addition, a framework from the LINSE Laboratory at the Universidad del Valle, Cali-Colombia, which was previously used by Riascos et al. [45], was used to test the U-FREI devices and the VOD devices. This framework was designed to simultaneously induce the boundary conditions of the experimental devices through horizontal and vertical actuator systems. Four cylindrical axes of 25.0 mm of diameter and a linear bearing allowed the vertical deformation of two U-FREI devices while they were compressed with a load constant of 19.0 kN, representing an average working gravity load of the reference structure for one of the experimental prototypes, as shown in Figure 3(a). The lateral deformation of the VOD and U-FREI devices during one of the tests was induced relative to each prototype. The operation of the framework is schematically shown in Figure 3(b).

3.3. Transfer System. The constant interaction between the numerical structure (NS) and experimental prototypes (ES) was realized using a horizontal transfer system (HTS), which replicated the reference signal originated from the dynamic response of the DOF of interest of the reference structure with a hybrid control system. The HTS was composed of a 45.0 kN hydraulic actuator guided by two 15.0 gpm servo valves and an internal linear variable differential transformer (LVDT). These components allowed the displacement of the piston to be measured with high accuracy, which was driven by a hydraulic pump with a maximum flow rate of 6.0 gpm. The transfer system inherently exhibits delay due to electronic latency and dynamic nonlinearities arising from phenomena such as friction in the actuator. To address this, a robust H_∞ controller was implemented to generate an optimal command signal to perform accurate HTS dynamic. This controller possesses the most optimal delay compensation achievable, inherent within its own properties. In addition, a Kalman filter was used to filter the noise in the signal measured by the LVDT, thereby increasing its accuracy in an estimated manner. More details of the controller and the Kalman filter used can be found in [45, 74–76].

The load acting on the U-FREI devices was induced by a vertical transfer system (VTS) consisting of a hydraulic power unit (HPU) and a vertical actuator connected to a load cell that measured the compression force. Due to the roll-out effects exhibited by U-FREI devices [70], a control system for the vertical actuator was implemented to maintain a constant load despite the variable deformation of the specimen during different deformation states in the simulation, as described in [45]. In this study, a servo valve, EATON KBS-10, was used to control an actuator with asymmetric behavior by implementing a proportional integral (PI) controller with constants k_p and k_i, which provides high accuracy in the behavior of the VTS. The controller loop

Table 1: Bouc–Wen model parameters for U-FREI devices.

b (kN/m)	c (kN · s/m)	a_1 (kN · m^{-3})	a_3 (kN · m^{-3})	a_5 (kN · m^{-3})	A (m)	β	Y	γ	n
$3.38 \cdot 10^3$	−4.59	−4.78	$3.12 \cdot 10^4$	$-1.21 \cdot 10^7$	1.00	613.30	1.92	762.10	1.00

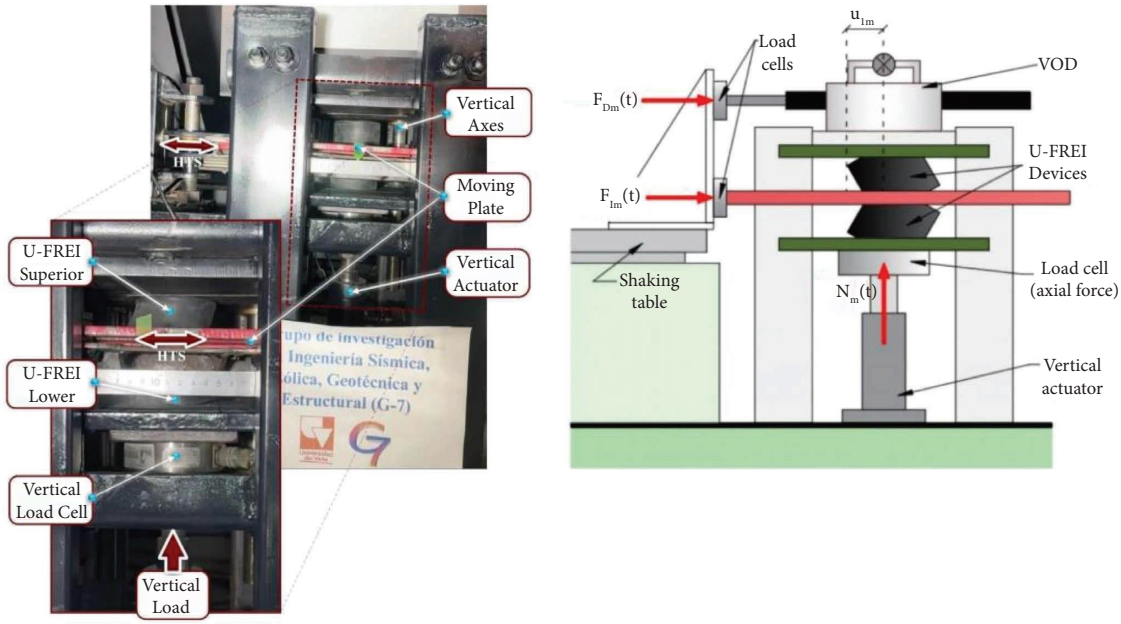

Figure 3: Framework of the experimental devices. (a) Experimental framework for testing U-FREI devices, and (b) scheme of operation of the framework for hybrid control system.

provides feedback from the normal restoring force, N_m, measured from the specimens, as shown in Figure 3(a).

3.4. Experimental Setups. An assessment of the reference structure with the hybrid control system was performed using five configuration schemes, as shown in Figure 4. These configuration diagrams describe how the numerical and experimental substructures and transfer systems are interconnected for the development of RTHS. In architecture no. 1 (AR. 1), the NS was subjected to an input signal corresponding to the base acceleration $\ddot{a_g}$, this responded to the excitation according to its dynamics properties and the performance of the hybrid control system. The response $u_1(t)$ was sent to the HTS, which replated $u_{1,m}(t)$ and transmitted it to the numerical model of the U-FREI and the experimental passive VOD devices under three opening conditions (10%, 50%, and 90%).

The opposing forces exerted by these prototypes, measured by the load cells, $F_{D,m}$ and $F_{I,a}$, were multiplied by the number of corresponding devices to obtain the total feedback forces F_D and F_I, which entered the numerical substructure and closed the loop. In this architecture, the performance of U-FREI devices is only numerical since there are no physical specimens. Architecture No. 2 (AR. 2) was similar to Architecture No. 1, where a pair of experimental U-FREI devices using the VTS were added, which applied a vertical load to the frame N_m, causing compression deformation of these specimens. This means that there are 2 U-FREI devices whose performance is calculated numerically through the Bouc–Wen model. Architecture no. 3 (AR. 3) removed the passive VOD devices used in architecture No. 2. Architecture no. 4 (AR. 4) was similar to the first configuration; however, the VOD devices exhibited semiactive behavior. Finally, architecture no. 5 (Ar. 5) replicates the second architecture using VOD devices in semiactive mode. These configurations were programmed in the Simulink software and executed with a SpeedGoat processor using a host computer with the Xpc protocol of MATLAB and a sampling frequency of 1024 Hz. SpeedGoat has a high processing capacity to guarantee real-time evaluation of the hybrid simulation.

3.5. Input Signal: Seismic Excitation (a_g). The seismic behavior of the hybrid control system as a dynamic vulnerability reduction system of the reference structure was assessed using RTHS tests with six internationally referenced seismic events: El Centro (USA, 1940), Loma Prieta (USA, 1989), Pizarro (Colombia, 2004), Chihuahua (Mexico, 2013), CAM (Italy, 1980), and CAT (Italy, 1980). All seismic events have a maximum acceleration of 0.981 m·s^{-2}, corresponding to 0.10 g, with a sample frequency of 1024 Hz equal to the RTHS run rate, as described in Section 3.4. The frequency

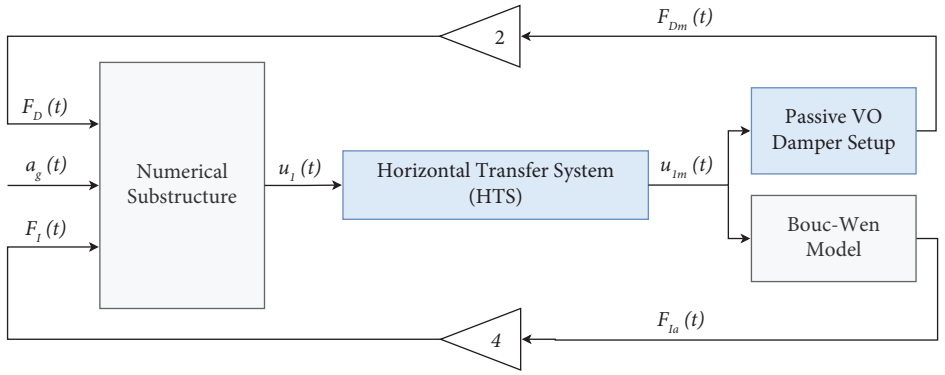

(a)

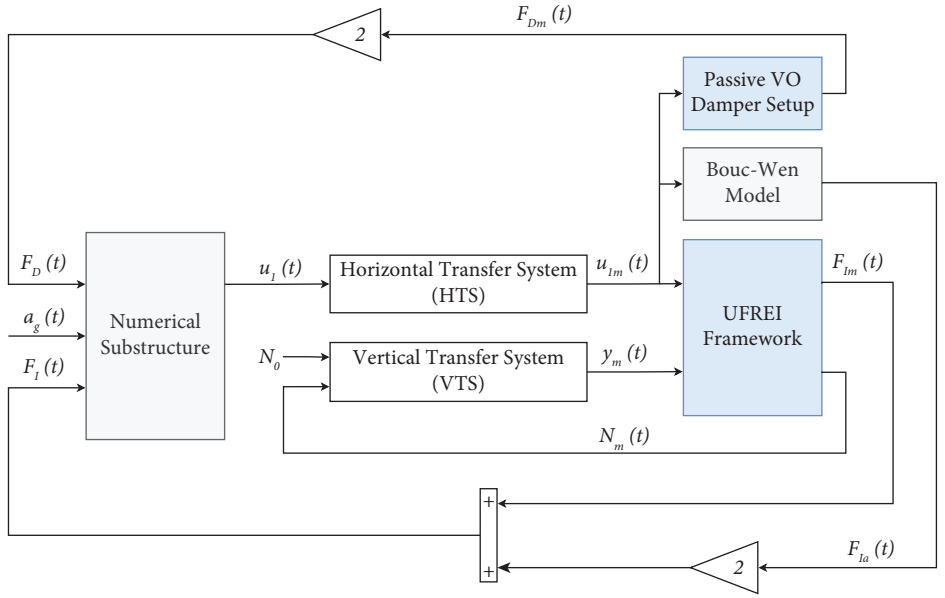

(b)

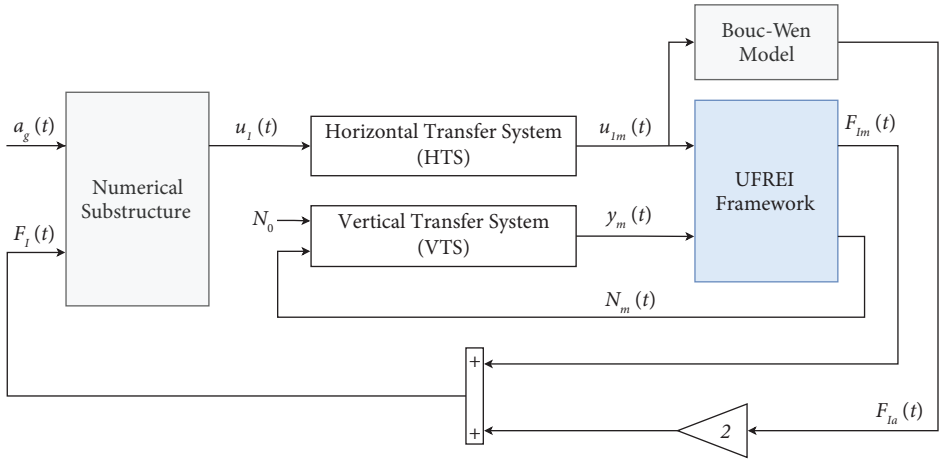

(c)

Figure 4: Continued.

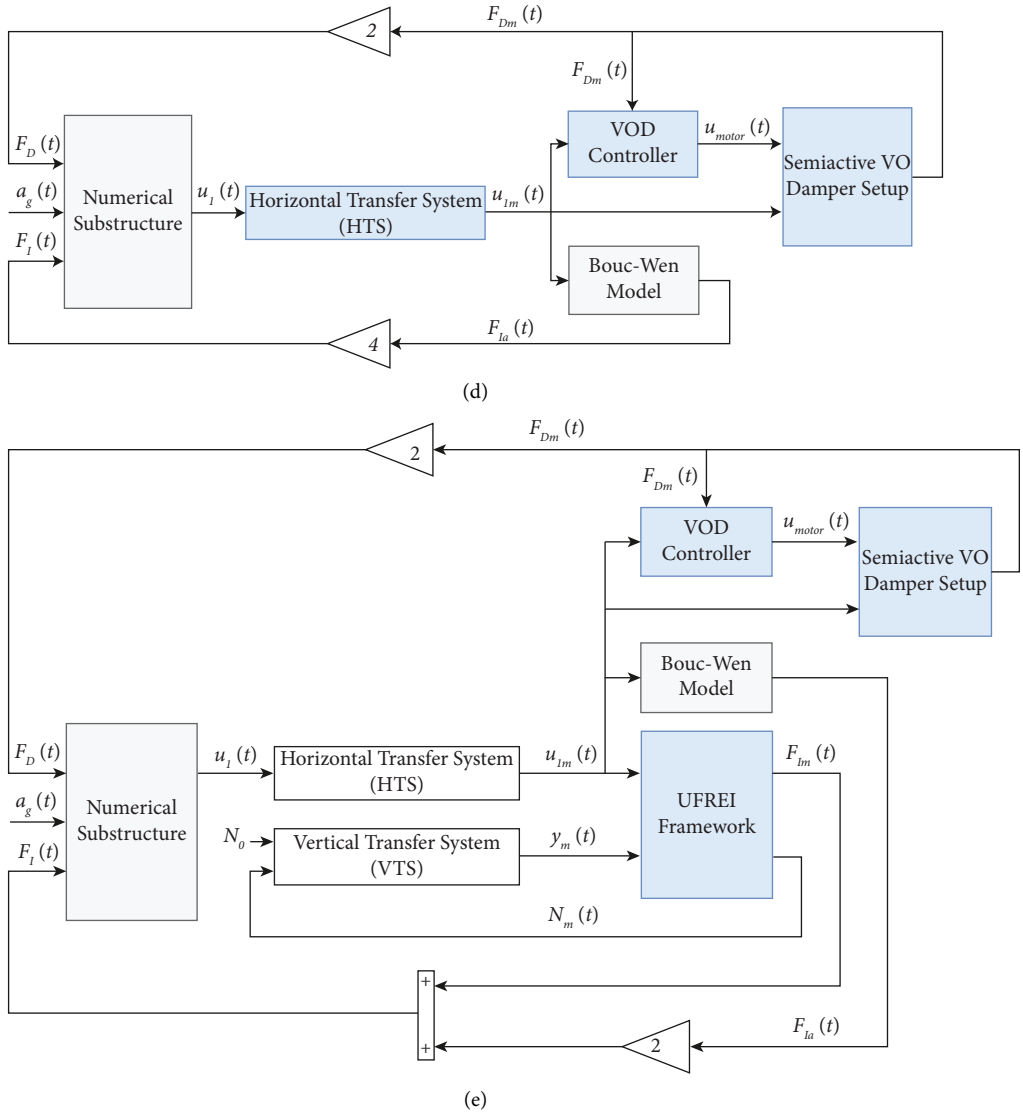

Figure 4: Configuration schemes. (a) Architecture no. 1, (b) architecture no. 2, (c) architecture no. 3, (d) architecture no. 4, and (e) architecture no. 5.

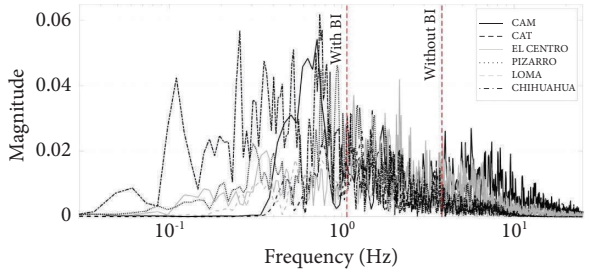

Figure 5: Frequency response of the assessed seismic events.

content of the evaluated earthquakes is shown in Figure 5. In addition, the graphical representation in the same figure demonstrates a reduction in the natural frequency of the entire structural system due to the influence of U-FREI devices.

4. Results and Discussion

4.1. Hybrid Control System Seismic Performance. The dynamic responses of the reference structure with the hybrid control system obtained for the five architecture setup described in Section 3.4, were compared with each other. This dynamic behavior, at level U_1, showed significant differences when architectures were used with experimental devices in comparison with numerical models for the seismic events assessed (Section 3.5), as shown in Figure 6. These discrepancies were due to the dynamics of the numerical model of the U-FREI devices (load F_I) and changes from the passive (closing 90%) to the semiactive state of the VOD devices. The numerical model achieved an effective damping coefficient (EDC) of approximately 4.0%, whereas the experimental specimens were close to 10.0% at low strain levels [77]. For this reason, architectures nos. 2 and 5 showed

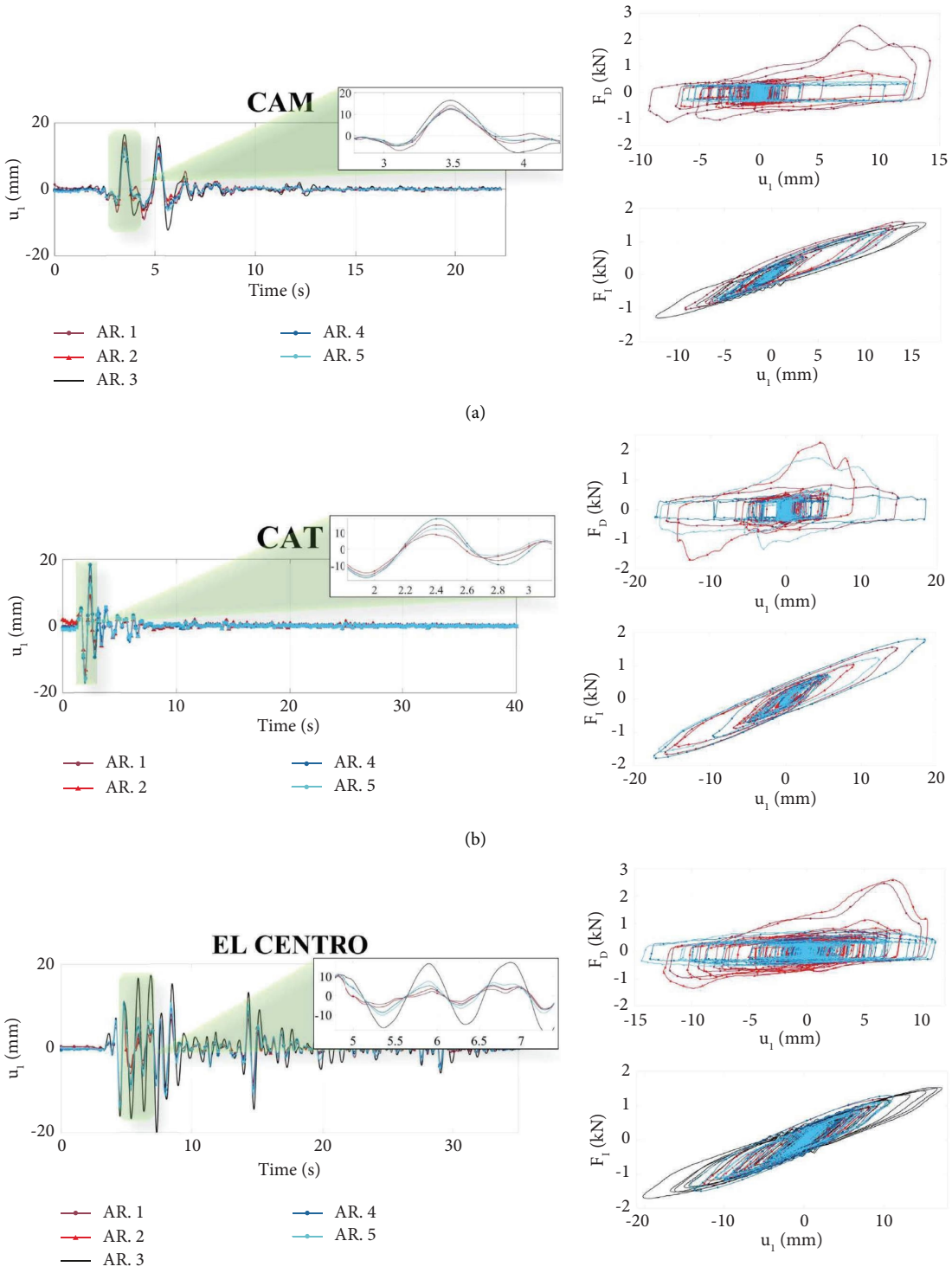

Figure 6: Continued.

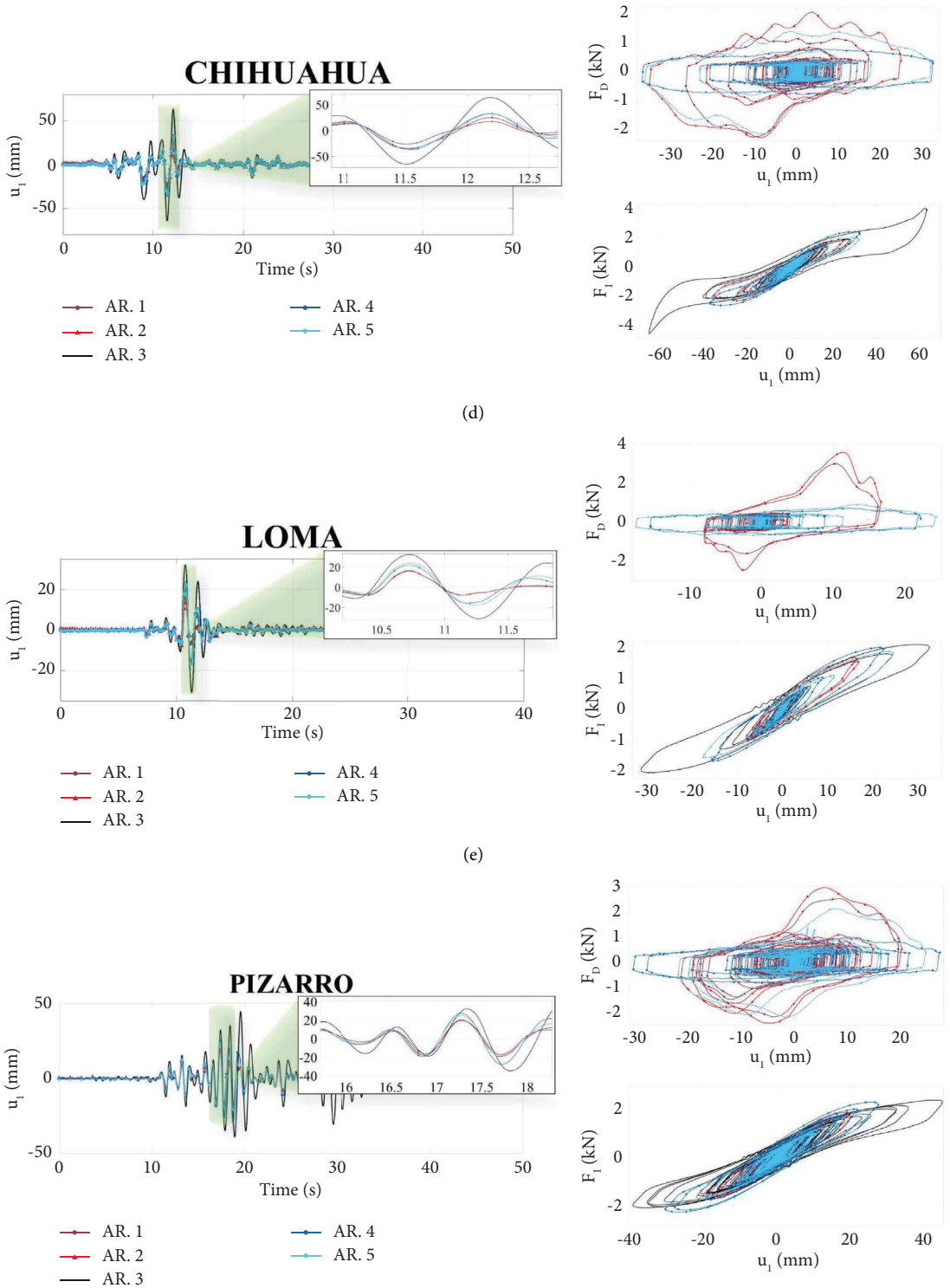

Figure 6: Base displacement (U_1) and hysteresis of the hybrid control system for all seismic event assessed in each architecture used.

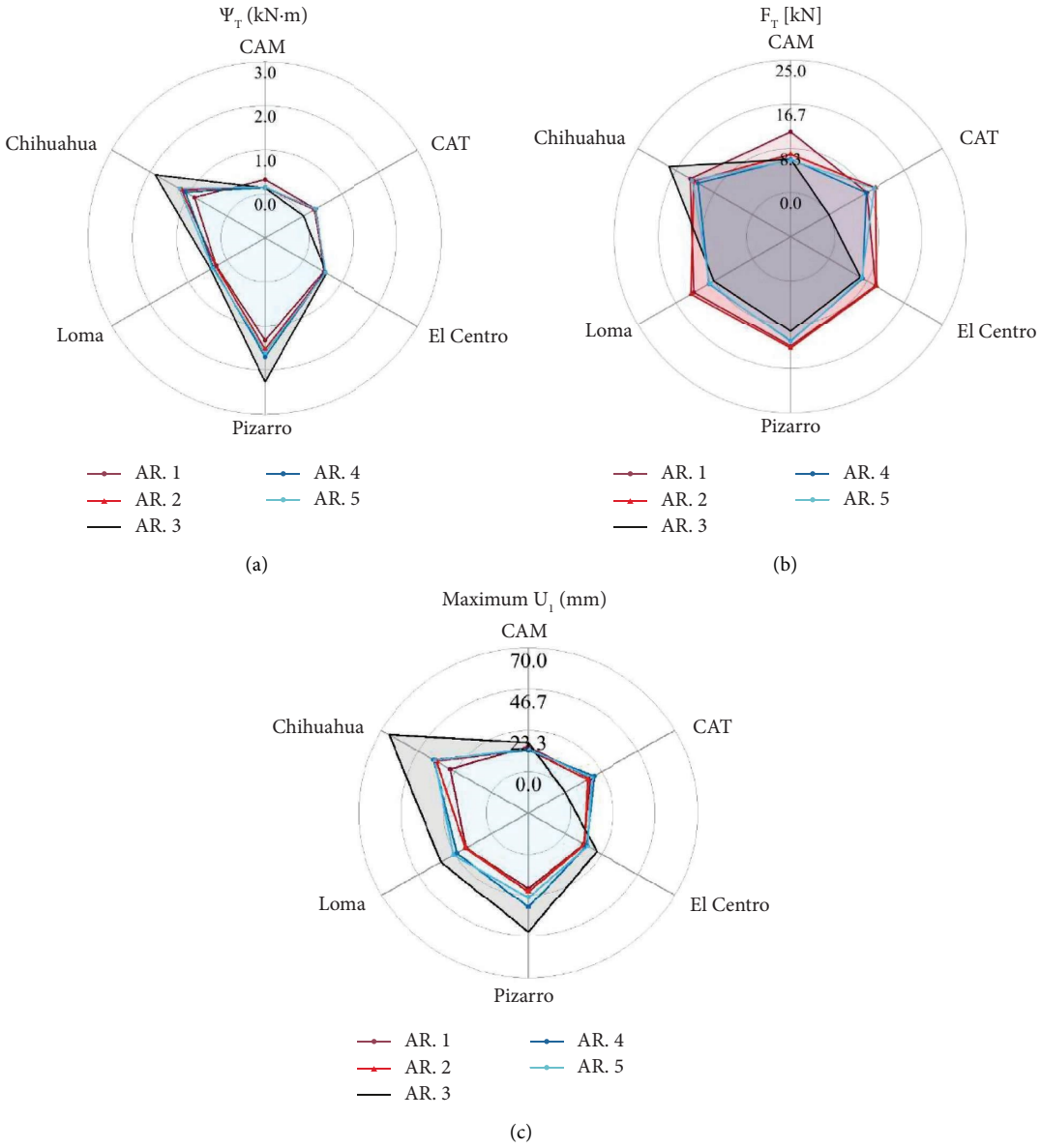

Figure 7: Energy dissipation capacity (a), total load of the hybrid control system (b), and maximum dynamic response U_1 (c).

a reduction in the displacement of level U_1 in comparison with architectures nos. 1 and 4, respectively, because experimental isolators provided more dissipation capacity to the system. Architecture no. 3 presents larger displacements and wider hysteresis curves for the U-FREI devices in comparison with the rest of architectures. In addition, an interaction was identified between the behavior of the U-FREI devices as a base isolator system and the dynamic performance of the VOD devices, which comprised the hybrid control system. The hysteresis curves of the U-FREI devices indicate consistent and reliable behavior during all tests by not reaching failure. The hysteresis curves of the VOD devices reveal that the force $F_{D,m}$ remains constant in architectures nos. 1 and 2, while exhibiting nonlinearity in architectures nos. 4 and 5. This behavior aligns with the passive and semiactive states of the VOD.

Dissipated energy (Ψ) is defined as the area under the hysteresis curve of a structural element, which is a crucial measure representing the ability of the system to absorb and dissipate energy during cyclic loads [78]. In this case, the total dissipated energy (Ψ_T) of the hybrid control system represents the sum of the energy dissipated by the U-FREI devices (Ψ_{UFREI}) combined with the energy dissipated by the VOD devices (Ψ_{VOD}). Ψ_T exhibited similar behavior in all states of the evaluated architectures. However, Architecture No. 3 (without VOD devices) presented an average increase in Ψ_T of 43.78%. Nevertheless, the dynamic performance of the hybrid control system (load F_T) generally induces a higher control force on the reference structure (up to 22.33% compared with Architecture No. 3), demonstrating a greater capacity for structural control, as shown in Figure 7(a). This control force allows a decrease in the dynamic

Table 2: Energy dissipation, total load of the hybrid control system, and maximum dynamic response U_1 for each architecture evaluated and for all seismic events used.

Earthquake		CAM	CAT	El Centro	Pizarro	Loma	Chihuahua
AR. 1	Ψ_T (kN·m)	0.326	0.314	0.532	1.333	0.273	0.842
	F_T (kN)	11.464	8.309	10.166	12.514	12.728	13.544
	Maximum U_1 (mm)	14.167	15.957	11.981	19.469	16.204	26.389
AR. 2	Ψ_T (kN·m)	0.142	0.284	0.561	1.536	0.291	1.177
	F_T (kN)	7.240	10.165	10.391	12.888	13.387	12.737
	Maximum U_1 (mm)	12.509	14.422	12.495	21.341	16.618	35.118
AR. 3	Ψ_T (kN·m)	0.133	—	0.599	2.270	0.423	1.869
	F_T (kN)	6.305	—	6.856	9.674	8.419	18.133
	Maximum U_1 (mm)	16.462	—	20.220	44.570	32.248	65.033
AR. 4	Ψ_T (kN·m)	0.142	0.321	0.563	1.706	0.346	1.078
	F_T (kN)	6.310	8.195	7.382	11.588	9.470	11.856
	Maximum U_1 (mm)	12.206	18.485	13.714	30.349	22.090	36.814
AR. 5	Ψ_T (kN·m)	0.153	0.310	0.577	1.611	0.368	1.240
	F_T (kN)	6.143	9.885	7.214	11.717	9.344	13.093
	Maximum U_1 (mm)	12.929	16.773	14.399	24.728	24.281	36.256

response of DOF U_1 of more than 35.49% compared with the structure with only U-FREI devices as base isolator system (Figure 7(b)). All these values were arranged in Table 2.

4.2. Reference Structure Seismic Performance with Hybrid Control System. The reference structure dynamic behavior was assessed in five architectures (Section 3.4) using VOD and U-FREI experimental devices as the hybrid control system and with the base fixed (through a numerical model). Each case was subjected to six seismic events described in Section 3.5. In the reference structure, the hybrid control systems generated a minimal reduction in the spectral response amplification factors of 78.57%, 85.33%, 40.82%, 85.12%, 63.89%, and 47.34% for the CAM, CAT, Chihuahua, El Centro, Loma Prieta, and Pizarro earthquakes, respectively, in comparison with the fixed reference structure, as shown in Figure 8. In addition, this figure also shows that the time-history response of DOF U_2 with the hybrid control system decreased with respect to the structure fixed for all seismic events evaluated.

U-FREI devices, as base isolator system, allow the reference structure to reduce its maximum drift by 60.53%, −1.96%, 75.09%, 32.08%, and 56.01%, respectively, for the CAM, Chihuahua, El Centro, Loma Prieta, and Pizarro seismic events compared to the fixed structure, as shown in Figure 9(a). Similarly, the hybrid control system in the passive state (90.0% closure) allowed the reference structure to reduce its maximum drift by 14.05%, −47.21%, 39.06%, 40.35%, and 23.35%, respectively, for the earthquakes compared with the response of the reference structure with only U-FREI devices. Furthermore, the hybrid control system in the semiactive state allowed the reference structure to reduce its maximum drift by 12.43%, 12.55%, 8.07%, 39.09%, 29.90%, and 6.16%, respectively, for the CAM, CAT, Chihuahua, El Centro, Loma Prieta, and Pizarro earthquakes compared with the response of the reference structure with the hybrid control system in the passive state (90.0% closure).

In brief, the maximum drift obtained for all evaluated architectures, including the 10.0%, 50.0%, and 90.0% valve-opening conditions for architectures 1 and 2, are shown in Figure 9(b). This figure quantifies the tendency of the hybrid control system in the semiactive state (architectures 4 and 5) to equal or improve up to 36.80% of the dynamic response of the structure when using only U-FREI devices as the base isolation system, compared to the response of the fixed structure. In addition, an increase in the maximum drift was observed when the passive-state hybrid control system with 90.0% opening was implemented in architectures 1 and 2 during seismic events compared to the fixed structure and a performance improvement of up to 15.50% was observed for this condition when the passive-state hybrid control system had a 10.0% opening. This observation shows that a passive control system does not guarantee a reduction in the drift for a seismic event with a wide frequency content; even, in some cases, it may cause an increase of the drift, with potential significant damage.

4.3. RTHS Performance. RTHS have errors owing to factors inherent to the evaluation methodology, such as DOF condensation in the numerical substructure, intrinsic noise in electronic signals of the ES and dynamics of the transfer systems, among others [79, 80]. To evaluate the accuracy of the RTHS, some indices have been proposed that consider the differences between the signals of references and measured at the interface of the substructure. The assessment of local performance relied on achieving synchronization in boundary conditions between the numerical response ($u^*_{i,d}$) transmitted to the actuator and the displacement attained in the physical component ($u^*_{i,m}$). This involves deriving a singular metric that signifies the disparity between actuator signals in the time domain. To facilitate comparison in the frequency domain, equations (9)–(13) were employed, corresponding to the frequency evaluation index (FEI). FEI compares the fast Fourier transform (FFT) of the desired signal $u^*_{i,d}$ with that of the measured signal $u^*_{i,m}$ at the

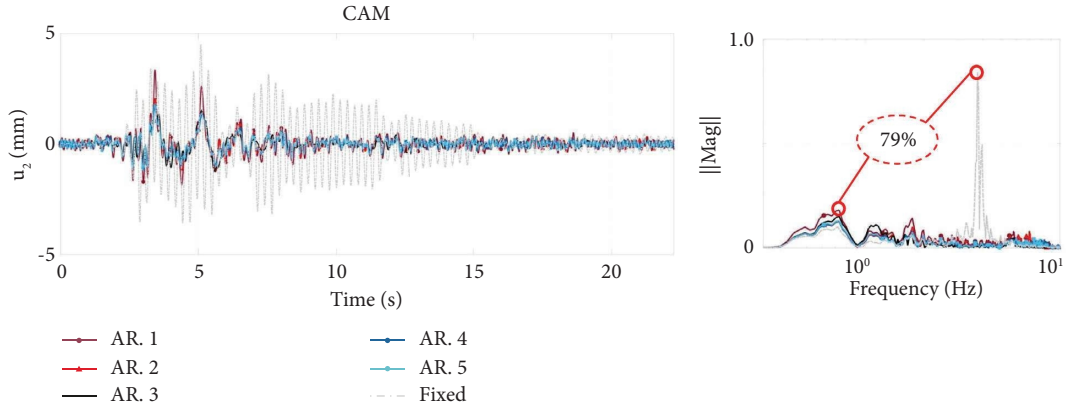

(a)

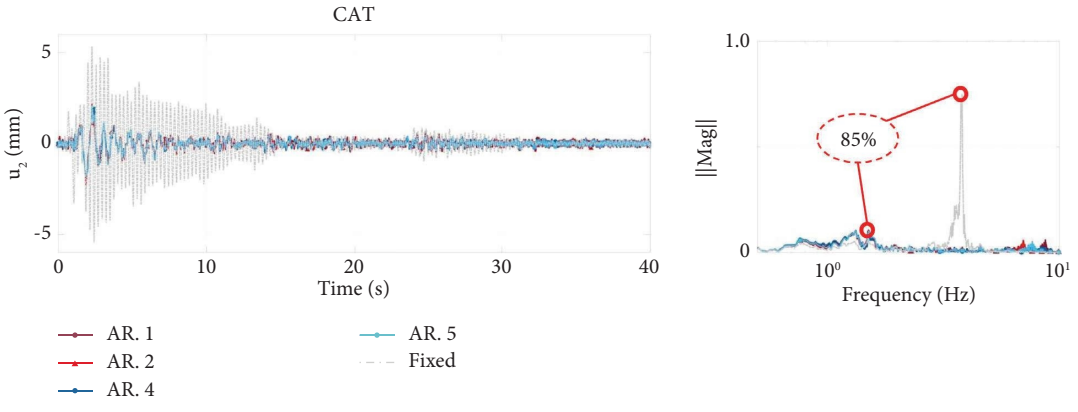

(b)

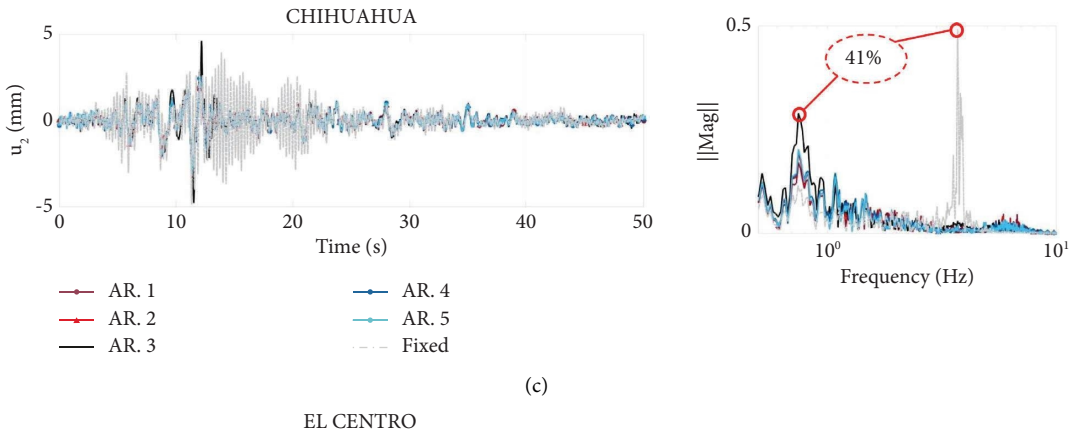

(c)

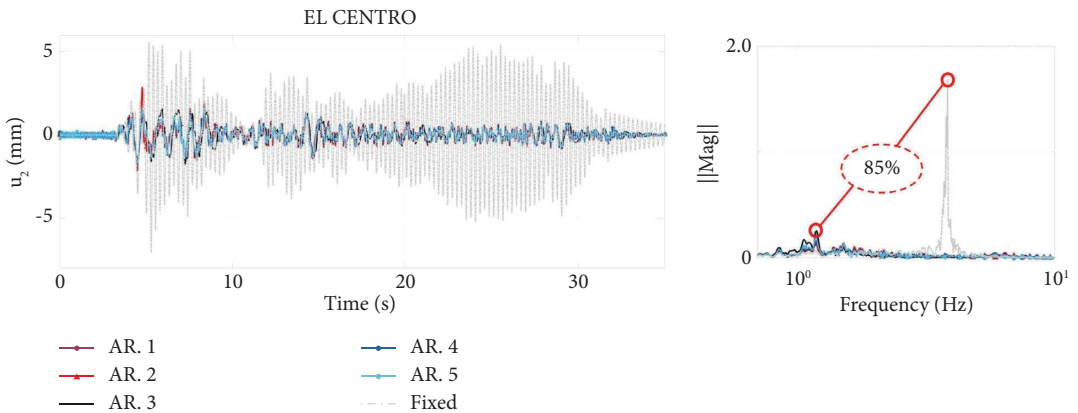

(d)

Figure 8: Continued.

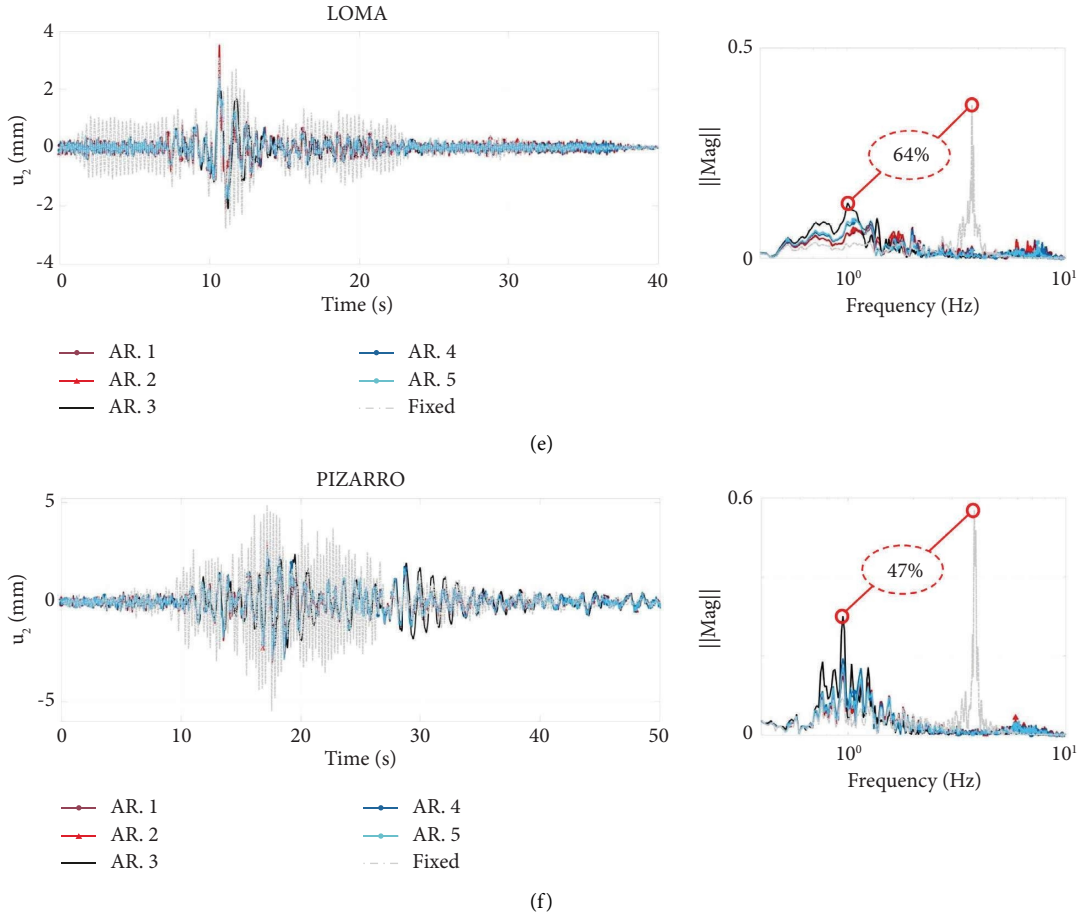

Figure 8: Dynamic response of the DOF U_2 for all test architectures.

actuator, considering parameters such as the dominant frequency during the RTHS denoted as f^{eq}, the generalized amplitude A_0, and the time delay δ, as described in [81].

$$\mathrm{FEI} = \sum_{j-1}^{N} \left(\frac{u^*_{i,m}(j)}{u^*_{i,d}(j)} \cdot \frac{\left\| u^*_{i,d}(j) \right\|^l}{\sum_{j-1}^{P} \left\| u^*_{i,d}(j) \right\|^l} \right), \tag{9}$$

$$f^{\mathrm{eq}} = \frac{\sum_{j-1}^{N} \left(\left\| u^*_{i,d}(j) \right\|^l \cdot f_i \right)}{\sum_{j-1}^{N} \left\| u^*_{i,d}(j) \right\|^l}, \tag{10}$$

$$A_0 = \|\mathrm{FEI}\|, \tag{11}$$

$$\emptyset = \arctan\left[\frac{Im(\mathrm{FEI})}{Re(\mathrm{FEI})} \right], \tag{12}$$

$$\delta = -\frac{\emptyset}{2 \cdot \pi \cdot f^{eq}}. \tag{13}$$

In addition, global indices account for the interaction between the numerical and experimental substructures. These were assessed within the time domain by quantifying the most substantial difference between the computed and observed displacements using e_{DM} and e_{MD}, as delineated in (14) and (15) [59, 82].

$$e_{\mathrm{DM}} = \frac{\left| \left| u^*_{i,d} \right|^{\max} - \left| u^*_{i,m} \right|^{\max} \right|}{\left| u^*_{i,m} \right|^{\max}}, \tag{14}$$

$$e_{\mathrm{MD}} = \frac{\left| u^*_{i,d} - u^*_{i,m} \right|^{\max}}{\left| u^*_{i,m} \right|^{\max}}. \tag{15}$$

All the indices were obtained for the five architectures used and are presented in Table 3. All cases presented a high level of horizontal tracking, with a generalized amplitude A_0 close to 1.0, and global errors lower than 6.80%, which allowed us to conclude that HTS has high performance and allows performing RTHS with a high level of accuracy.

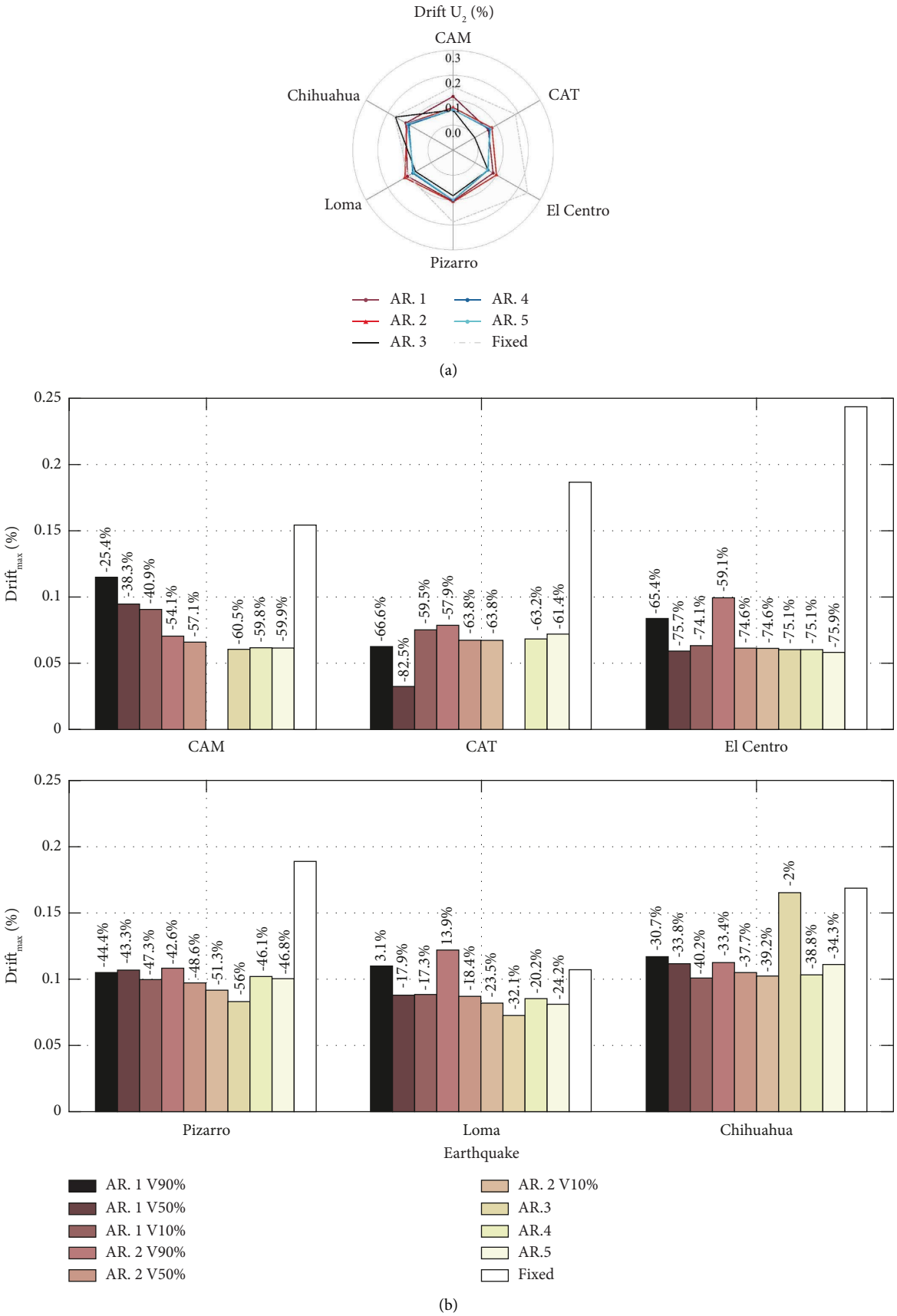

Figure 9: Structure drift performance for all test architectures.

Table 3: RTHS assessment indexes.

Transfer system	Earthquake	FEI	f_{eq} (Hz)	A_0	e_{DM} (%)	e_{MD} (%)	δ (ms)
*Architecture no. 1**							
HTS	El Centro	0.988−0.03i	1.358	0.988	5.120	6.791	3.146
	Loma P.	1.018−0.02i	1.079	1.018	1.859	3.182	2.194
	Pizarro	0.980−0.02i	1.038	0.980	1.711	2.903	2.465
	Chihuahua	0.996−0.01i	0.754	0.996	0.977	1.880	2.135
	CAM	1.065−0.02i	0.776	1.065	3.525	5.515	4.173
	CAT	0.937−0.02i	1.118	0.938	2.649	6.183	2.952
*Architecture no. 2**							
HTS	El Centro	0.982−0.02i	1.308	0.982	3.597	6.048	2.813
	Loma P.	1.027−0.01i	0.736	1.027	1.968	2.808	2.011
	Pizarro	1.012−0.01i	0.908	1.012	0.976	3.265	2.488
	Chihuahua	1.009−0.01i	0.663	1.009	0.535	1.652	1.954
	CAM	0.931−0.01i	0.633	0.931	1.954	3.752	3.889
	CAT	1.062−0.01i	0.699	1.062	1.909	3.782	2.344
Architecture no. 3							
HTS	El Centro	0.981−0.02i	1.118	0.982	2.549	5.044	2.959
	Loma P.	0.991−0.02i	0.934	0.992	1.381	3.483	3.487
	Pizarro	0.993−0.01i	0.934	0.993	0.849	2.156	1.628
	Chihuahua	0.997−0.00i	0.722	0.997	0.639	1.728	0.935
	CAM	0.952−0.02i	0.832	0.953	3.315	5.237	4.015
	CAT	—	—	—	—	—	—
Architecture no. 4							
HTS	El Centro	0.953−0.03i	1.145	0.953	2.880	5.990	3.681
	Loma P.	0.986−0.01i	0.941	0.986	0.606	2.471	1.556
	Pizarro	0.999−0.01i	1.025	0.999	1.022	3.285	2.084
	Chihuahua	0.998−0.01i	0.780	0.998	0.535	1.759	1.785
	CAM	1.006−0.01i	0.854	1.006	1.340	2.771	2.743
	CAT	0.982−0.01i	1.082	0.982	1.496	2.857	1.581
Architecture no. 5							
HTS	El Centro	0.982−0.02i	1.177	0.982	1.402	5.470	2.613
	Loma P.	0.998−0.01i	0.995	0.998	0.793	2.229	1.784
	Pizarro	0.984−0.01i	0.859	0.984	1.133	2.661	2.223
	Chihuahua	0.994−0.01i	0.690	0.994	0.713	2.046	2.083
	CAM	0.886−0.01i	0.624	0.886	3.773	5.306	2.930
	CAT	0.900−0.01i	0.668	0.900	3.615	5.776	1.592

*Valve with 90.0% opening.

5. Conclusions

In this study, the assessment of the seismic behavior of a low-degree-of-freedom reference structure with a hybrid control system composed of unconnected fiber-reinforced elastomeric isolator (U-FREI) and variable orifice dampers (VOD) devices was performed using the RTHS methodology for six seismic events: CAT, CAM, El Centro, Loma Prieta, Chihuahua, and Pizarro, scaled to an acceleration of 0.10 g ($0.981\ m{\cdot}s^{-2}$). In addition, five architectures were evaluated for these seismic events, including a numerical model (Bouc–Wen model) of the U-FREI devices for two test architectures, which had an effective damping coefficient in the experimental base isolation system (EDC≈10.0%) higher than that used in the numerical model (EDC≈4.0%), presenting differences between architectures 1-2 and 4-5.

The architecture no. 3 without VOD devices presented an increase in the energy dissipation capacity (Ψ_T) of the hybrid control system of 43.78%. In addition, the induced control load (F_T) was higher in the reference structure by up to 22.33% compared with architecture no. 3. Furthermore, this control load reduces the response of the DOF U_1 by more than 35.49% compared to the structure with only U-FREI devices.

The hybrid control system for all architectures generated, in the reference structure, a minimal reduction in the spectral response amplification factor of 78.57%, 85.33%, 40.82%, 85.12%, 63.89%, and 47.34% for CAM, CAT, Chihuahua, El Centro, Loma Prieta, and Pizarro earthquakes, respectively, in comparison with the reference structure fixed. Similarly, U-FREI devices as base isolator system allow the reference structure to reduce its maximum drift by 60.53%, −1.96%, 75.09%, 32.08%, and 56.01%, respectively, for the evaluated earthquakes (without CAT) compared with the fixed structure. Likewise, the hybrid control system in the passive state (90.0% closure) allowed the reference structure to reduce its maximum drift by 14.05%, −47.21%, 39.06%, 40.35%, and 23.35%, respectively,

for the evaluated earthquakes (without CAT) compared with the response of the reference structure with only U-FREI devices. Furthermore, the hybrid control system in the semiactive state allows the reference structure to reduce its maximum drift by 12.43%, 12.55%, 8.07%, 39.09%, 29.90%, and 6.16%, respectively, for the evaluated earthquakes compared to the response of the reference structure with the hybrid control system in the passive state (90.0% closure). This demonstrates the dynamic robustness of the hybrid control system in the semiactive condition to decrease base displacements and maintain maximum floor drifts under minimum conditions. The results position this study as one of the first tests of the technical potential of a hybrid control system composed of smart base isolation with U-FREI and VOD devices to reduce the seismic vulnerability of low-degree-of-freedom reference structures.

The experimental assessment was performed using the RTHS methodology, with a simplified 2-DOF model of the reference structure as a numerical substructure and U-FREI and VOD devices as a hybrid control system as an experimental substructure. For the tracking levels of the horizontal transfer systems, all cases presented high-level tracking, with a generalized amplitude A_0 close to 1.0 and global errors lower than 6.79%. Furthermore, HTS had delays of less than 4.17 ms, employing a robust H_∞ controller in all cases. The above results indicate that the RTHS exhibits high fidelity and accuracy.

Data Availability

The data that support the findings of this study are available from the corresponding author upon reasonable request.

Disclosure

This work is part of the research project: Real-time hybrid simulations: a reliable, fast, and economical alternative for the evaluation of resilient structures, under the program: Emerging technologies for the mitigation of seismic risk in civil infrastructure, CT 463-2020 – program code 110685270483.

Conflicts of Interest

The authors declare that there are no conflicts of interest.

Authors' Contributions

All authors contributed to this research and discussed the results and reviews during all phases of the research paper. All authors read and accepted the published version of the research paper.

Acknowledgments

The authors would like to express their gratitude to the Universidad del Valle and the Ministerio de Ciencia Tecnología e Innovación (Minciencias), entities that financed the project.

References

[1] S. D. K. U. P. Priya and N. R. Iyer, "Enhancing the seismic response of buildings with energy dissipation methods-an overview," *Journal of Civil Engineering Research*, vol. 2014, pp. 17–22, 2014.

[2] N. Torunbalci, "Seismic isolation and energy dissipating systems in earthquake resistant design," in *Proceedings of the 13th World conference on earthquake engineering*, Vancouver, Canada, December 2004.

[3] B. Akbaş and J. Shen, "Earthquake resistant design and energy concepts," *Technical Journal of Turkish Chamber of Civil Engineers*, vol. 14, pp. 2877–2901, 2003.

[4] T. T. Soong and B. F. Spencer, "Supplemental energy dissipation: state-of-the-art and state-of-the-practice," *Engineering Structures*, vol. 24, no. 3, pp. 243–259, 2002.

[5] I. E. Madera Sierra, D. Losanno, S. Strano, J. Marulanda, and P. Thomson, "Development and experimental behavior of HDR seismic isolators for low-rise residential buildings," *Engineering Structures*, vol. 183, pp. 894–906, 2019.

[6] D. De Domenico, D. Losanno, and N. Vaiana, "Experimental tests and numerical modeling of full-scale unbonded fiber reinforced elastomeric isolators (UFREIs) under bidirectional excitation," *Engineering Structures*, vol. 274, Article ID 115118, 2023.

[7] A. B. Habieb, A. Formisano, G. Milani, and G. Pianese, "Seismic performance of Unbonded Fiber-Reinforced Elastomeric Isolators (UFREI) made by recycled rubber. Influence of suboptimal crosslinking," *Engineering Structures*, vol. 256, Article ID 114038, 2022.

[8] S. Prakash and R. S. Jangid, "Seismic response of isolated structures with an improved model of the UFREI," *Structures*, vol. 42, pp. 434–448, 2022.

[9] M. C. Constantinou and M. D. Symans, "Experimental study of seismic response of buildings with supplemental fluid dampers," *The Structural Design of Tall Buildings*, vol. 2, pp. 93–132, 1993.

[10] Z. Yang, Y. L. Xu, and X. L. Lu, "Experimental seismic study of adjacent buildings with fluid dampers," *Journal of Structural Engineering*, vol. 129, no. 2, pp. 197–205, 2003.

[11] H. H. Lee and C.-S. Tsai, "Analytical model of viscoelastic dampers for seismic mitigation of structures," *Computers & Structures*, vol. 50, no. 1, pp. 111–121, 1994.

[12] S. Bagheri, M. Barghian, F. Saieri, and A. Farzinfar, "U-shaped metallic-yielding damper in building structures: seismic behavior and comparison with a friction damper," *Structures*, vol. 3, pp. 163–171, 2015.

[13] L. M. Moreschi and M. P. Singh, "Design of yielding metallic and friction dampers for optimal seismic performance," *Earthquake Engineering & Structural Dynamics*, vol. 32, no. 8, pp. 1291–1311, 2003.

[14] B.-S. Kang, G.-J. Kang, and B.-Y. Moon, "Hole and lead plug effect on fiber reinforced elastomeric isolator for seismic isolation," *Journal of Materials Processing Technology*, vol. 140, no. 1-3, pp. 592–597, 2003.

[15] J. M. Kelly, "Analysis of fiber-reinforced elastomeric isolators," *Journal of Seismology and Earthquake Engineering*, vol. 2, pp. 19–34, 1999.

[16] D. Losanno, I. E. Madera Sierra, M. Spizzuoco, J. Marulanda, and P. Thomson, "Experimental assessment and analytical modeling of novel fiber-reinforced isolators in unbounded

configuration," *Composite Structures*, vol. 212, pp. 66–82, 2019.

[17] D. Losanno, I. E. Madera Sierra, M. Spizzuoco, J. Marulanda, and P. Thomson, "Experimental performance of unbonded polyester and carbon fiber reinforced elastomeric isolators under bidirectional seismic excitation," *Engineering Structures*, vol. 209, Article ID 110003, 2020.

[18] C. Zhang and J. Ou, "Control structure interaction of electromagnetic mass damper system for structural vibration control," *Journal of Engineering Mechanics*, vol. 134, no. 5, pp. 428–437, 2008.

[19] D.-H. Yang, J.-H. Shin, H. Lee, S.-K. Kim, and M. K. Kwak, "Active vibration control of structure by active mass damper and multi-modal negative acceleration feedback control algorithm," *Journal of Sound and Vibration*, vol. 392, pp. 18–30, 2017.

[20] M. Yamamoto, S. Aizawa, M. Higashino, and K. Toyama, "Practical applications of active mass dampers with hydraulic actuator," *Earthquake Engineering & Structural Dynamics*, vol. 30, no. 11, pp. 1697–1717, 2001.

[21] G. Song, J. Lin, F. W. Williams, and Z. Wu, "Precise integration strategy for aseismic LQG control of structures," *International Journal for Numerical Methods in Engineering*, vol. 68, no. 12, pp. 1281–1300, 2006.

[22] R. E. Christenson, B. F. Spencer, N. Hori, and K. Seto, "Coupled building control using acceleration feedback," *Computer-Aided Civil and Infrastructure Engineering*, vol. 18, no. 1, pp. 4–18, 2003.

[23] S. L. Djajakesukma, B. Samali, and H. Nguyen, "Study of a semi-active stiffness damper under various earthquake inputs," *Earthquake Engineering & Structural Dynamics*, vol. 31, no. 10, pp. 1757–1776, 2002.

[24] M. D. Symans and M. C. Constantinou, "Seismic testing of a building structure with a semi-active fluid damper control system," *Earthquake Engineering & Structural Dynamics*, vol. 26, no. 7, pp. 759–777, 1997.

[25] G. J. Hiemenz, Y. T. Choi, and N. M. Wereley, "Seismic control of civil structures utilizing semi–active MR braces," *Computer-Aided Civil and Infrastructure Engineering*, vol. 18, no. 1, pp. 31–44, 2003.

[26] E. Renzi and G. Serino, "Testing and modelling a semi-actively controlled steel frame structure equipped with MR dampers," *Structural Control and Health Monitoring*, vol. 11, no. 3, pp. 189–221, 2004.

[27] Y. Kim, R. Langari, and S. Hurlebaus, "Semiactive nonlinear control of a building with a magnetorheological damper system," *Mechanical Systems and Signal Processing*, vol. 23, no. 2, pp. 300–315, 2009.

[28] S.-P. Chang, N. Makris, A. S. Whittaker, and A. C. T. Thompson, "Experimental and analytical studies on the performance of hybrid isolation systems," *Earthquake Engineering & Structural Dynamics*, vol. 31, no. 2, pp. 421–443, 2002.

[29] M.-C. Hsieh, G.-L. Huang, H. Liu, S.-J. Chen, and B.-F. Chen, "A numerical study of hybrid tuned mass damper and tuned liquid damper system on structure motion control," *Ocean Engineering*, vol. 242, Article ID 110129, 2021.

[30] A. H. Deringöl and E. M. Güneyisi, "Influence of nonlinear fluid viscous dampers in controlling the seismic response of the base-isolated buildings," *Structures*, vol. 34, pp. 1923–1941, 2021.

[31] X. Chen and J. Xiong, "Seismic resilient design with base isolation device using friction pendulum bearing and viscous damper," *Soil Dynamics and Earthquake Engineering*, vol. 153, Article ID 107073, 2022.

[32] R. Dey and P. Saha, "Seismic response control of smart base-isolated benchmark building using hybrid control strategy (viscous fluid damper with MR damper)," in *Recent Advances in Structural Engineering*, A. R. M. Rao and K. Ramanjaneyulu, Eds., pp. 365–374, Springer, Singapore, 2019.

[33] M. Mohebbi, M. Noruzvand, H. Dadkhah, and K. Shakeri, "Direct displacement-based design approach for isolated structures equipped with supplemental fluid viscous damper," *Journal of Building Engineering*, vol. 45, Article ID 103684, 2022.

[34] Y. Liu, J. Wu, and M. Donà, "Effectiveness of fluid-viscous dampers for improved seismic performance of inter-storey isolated buildings," *Engineering Structures*, vol. 169, pp. 276–292, 2018.

[35] B. Chen, Y.-Z. Sun, Y.-L. Li, and S.-L. Zhao, "Control of seismic response of a building frame by using hybrid system with magnetorheological dampers and isolators," *Advances in Structural Engineering*, vol. 17, no. 8, pp. 1199–1215, 2014.

[36] N. Wongprasert and M. D. Symans, "Experimental evaluation of adaptive elastomeric base-isolated structures using variable-orifice fluid dampers," *Journal of Structural Engineering*, vol. 131, no. 6, pp. 867–877, 2005.

[37] B.-Y. Moon, G.-J. Kang, B.-S. Kang, and J. M. Kelly, "Design and manufacturing of fiber reinforced elastomeric isolator for seismic isolation," *Journal of Materials Processing Technology*, vol. 130–131, pp. 145–150, 2002.

[38] B.-S. Kang, L. Li, and T.-W. Ku, "Dynamic response characteristics of seismic isolation systems for building structures," *Journal of Mechanical Science and Technology*, vol. 23, no. 8, pp. 2179–2192, 2009.

[39] J. M. Kelly and D. Konstantinidis, *Mechanics of Rubber Bearings for Seismic and Vibration Isolation*, John Wiley & Sons, Hoboken, NW, USA, 2011.

[40] M. Pauletta, A. Cortesia, and G. Russo, "Roll-out instability of small size fiber-reinforced elastomeric isolators in unbonded applications," *Engineering Structures*, vol. 102, pp. 358–368, 2015.

[41] M. Pauletta, A. Cortesia, I. Pitacco, and G. Russo, "A new bilinear constitutive shear relationship for Unbonded Fiber-Reinforced Elastomeric Isolators (U-FREIs)," *Composite Structures*, vol. 168, pp. 725–738, 2017.

[42] M. Pauletta, F. Pinzano, G. Frappa, and G. Russo, "Tensile tests for the improvement of adhesion between rubber and steel layers in elastomeric isolators," *Applied Sciences*, vol. 10, no. 22, pp. 8063–8118, 2020.

[43] M. Spizzuoco, A. Calabrese, and G. Serino, "Innovative low-cost recycled rubber–fiber reinforced isolator: experimental tests and Finite Element Analyses," *Engineering Structures*, vol. 76, pp. 99–111, 2014.

[44] D. Losanno, M. Spizzuoco, and A. Calabrese, "Bidirectional shaking-table tests of unbonded recycled-rubber fiber-reinforced bearings (RR-FRBs)," *Structural Control and Health Monitoring*, vol. 26, no. 9, p. e2386, 2019.

[45] C. Riascos, S. Klopov, D. Losanno, J. Marulanda, and P. Thomson, "Real-time hybrid simulations including rocking effects: the case of a frame-structure with unbounded elastomeric isolators," *Structural Control and Health Monitoring*, vol. 29, no. 9, p. e2984, 2022.

[46] D. Losanno, N. Ravichandran, F. Parisi, A. Calabrese, and G. Serino, "Seismic performance of a Low-Cost base isolation system for unreinforced brick Masonry buildings in

developing countries," *Soil Dynamics and Earthquake Engineering*, vol. 141, Article ID 106501, 2021.

[47] A. Calabrese, D. Losanno, M. Spizzuoco, S. Strano, and M. Terzo, "Recycled Rubber Fiber Reinforced Bearings (RR-FRBs) as base isolators for residential buildings in developing countries: the demonstration building of Pasir Badak, Indonesia," *Engineering Structures*, vol. 192, pp. 126–144, 2019.

[48] H. Yoshioka, J. C. Ramallo, and B. F. Spencer, "Smart base isolation strategies employing magnetorheological dampers," *Journal of Engineering Mechanics*, vol. 128, no. 5, pp. 540–551, 2002.

[49] P.-C. Chen, K.-C. Tsai, and P.-Y. Lin, "Real-time hybrid testing of a smart base isolation system," *Earthquake Engineering & Structural Dynamics*, vol. 43, no. 1, pp. 139–158, 2014.

[50] H. Ghaffarzadeh, E. A. Dehrod, and N. Talebian, "Semi-active fuzzy control for seismic response reduction of building frames using variable orifice dampers subjected to near-fault earthquakes," *Journal of Vibration and Control*, vol. 19, no. 13, pp. 1980–1998, 2013.

[51] A. Tsipianitis and Y. Tsompanakis, "Multi-objective optimization of base-isolated tanks with supplemental linear viscous dampers," *Infrastructure*, vol. 7, no. 11, p. 157, 2022.

[52] J.-Y. Li and S. Zhu, "Advanced vibration isolation technique using versatile electromagnetic shunt damper with tunable behavior," *Engineering Structures*, vol. 242, Article ID 112503, 2021.

[53] L.-Y. Lu and G.-L. Lin, "Fuzzy friction controllers for semi-active seismic isolation systems," *Journal of Intelligent Material Systems and Structures*, vol. 20, no. 14, pp. 1747–1770, 2009.

[54] M. Nakashima, H. Kato, and E. Takaoka, "Development of real-time pseudo dynamic testing," *Earthquake Engineering & Structural Dynamics*, vol. 21, no. 1, pp. 79–92, 1992.

[55] K. Takanashi, K. Udagawa, M. Seki, T. Okada, and H. Tanaka, "Nonlinear earthquake response analysis of structures by a computer-actuator on-line system," *Bulletin of Earthquake Resistant Structure Research Center*, vol. 8, pp. 1–17, 1975.

[56] T. Simpson, V. K. Dertimanis, and E. N. Chatzi, "Towards data-driven real-time hybrid simulation: adaptive modeling of control plants," *Front Built Environ*, vol. 6, 2020.

[57] M. Nakashima, "Hybrid simulation: an early history," *Earthquake Engineering & Structural Dynamics*, vol. 49, no. 10, pp. 949–962, 2020.

[58] A. Maghareh, A. I. Ozdagli, and S. J. Dyke, "Modeling and implementation of distributed real-time hybrid simulation," in *Proceedings of the 10th National Conference in Earthquake Engineering, Earthquake Engineering Research Institute*, Anchorage, AK, USA, August 2014.

[59] C. E. Silva, D. Gomez, A. Maghareh, S. J. Dyke, and B. F. Spencer, "Benchmark control problem for real-time hybrid simulation," *Mechanical Systems and Signal Processing*, vol. 135, Article ID 106381, 2020.

[60] I. Lanese, A. Pavese, and M. Furinghetti, "Hybrid testing of seismic isolated structures: facing time and geometry scaling issues," in *Proceedings of the 1st European Conference on Earthquake Engineering*, pp. 19–21, Thessaloniki, Greece, January 2018.

[61] N. Nakata, R. Erb, and M. Stehman, "Mixed force and displacement control for testing base-isolated bearings in real-time hybrid simulation," *Journal of Earthquake Engineering*, vol. 23, no. 6, pp. 1055–1071, 2019.

[62] T. Asai, C.-M. Chang, B. M. Phillips, and B. F. Spencer, "Real-time hybrid simulation of a smart outrigger damping system for high-rise buildings," *Engineering Structures*, vol. 57, pp. 177–188, 2013.

[63] B. M. Phillips, Y. Chae, Z. Jiang, B. F. Spencer, J. M. Ricles, and R. Christenson, "Real-time hybrid simulation benchmark study with a large-scale MR damper," in *Proceedings of the 5th World Conference of the International Association for Structural Control and Monitoring*, pp. 12–14, Barcelona, Spain, July 2010.

[64] Z. Jiang, S. J. Kim, S. Plude, and R. Christenson, "Real-time hybrid simulation of a complex bridge model with MR dampers using the convolution integral method," *Smart Materials and Structures*, vol. 22, no. 10, Article ID 105008, 2013.

[65] R. Christenson, Y. Z. Lin, A. Emmons, and B. Bass, "Large-scale experimental verification of semiactive control through real-time hybrid simulation," *Journal of Structural Engineering*, vol. 134, no. 4, pp. 522–534, 2008.

[66] C. Chen and J. M. Ricles, "Large-scale real-time hybrid simulation involving multiple experimental substructures and adaptive actuator delay compensation," *Earthquake Engineering & Structural Dynamics*, vol. 41, no. 3, pp. 549–569, 2012.

[67] R. Christenson and Y. Z. Lin, "Real-time hybrid simulation of a seismically excited structure with largescale magneto-rheological fluid dampers," *Hybrid Simulation Theory, Implementations and Applications*, vol. 15, 2008.

[68] X. Shao and C. Griffith, "An overview of hybrid simulation implementations in NEES projects," *Engineering Structures*, vol. 56, pp. 1439–1451, 2013.

[69] G. Magliulo, "Shake table tests on infill plasterboard partitions," *The Open Construction & Building Technology Journal*, vol. 6, no. 1, pp. 155–163, 2012.

[70] A. Calabrese, S. Strano, and M. Terzo, "Real-time hybrid simulations vs shaking table tests: case study of a fibre-reinforced bearings isolated building under seismic loading," *Structural Control and Health Monitoring*, vol. 22, no. 3, pp. 535–556, 2015.

[71] A. Calabrese, M. Spizzuoco, G. Serino, G. Della Corte, and G. Maddaloni, "Shaking table investigation of a novel, low-cost, base isolation technology using recycled rubber," *Structural Control and Health Monitoring*, vol. 22, no. 1, pp. 107–122, 2015.

[72] B. D. O. Anderson and J. B. Moore, *Optimal Control: Linear Quadratic Methods*, Dover Publications, Mineola, NY, USA, 2007.

[73] A. Manzoori and H. Toopchi-Nezhad, "Application of an extended bouc-wen model in seismic response prediction of unbonded fiber-reinforced isolators," *Journal of Earthquake Engineering*, vol. 21, no. 1, pp. 87–104, 2017.

[74] C. Riascos, J. Marulanda Casas, and P. Thomson, "Semi-active tuned liquid column damper implementation with real-time hybrid simulations," *SPIE Proceedings*, vol. 9799, Article ID 979919, 2016.

[75] C. A. Riascos-González, P. Thomson, and S. Dyke, "Evaluación del desempeño de un amortiguador de masa sintonizado no lineal mediante simulaciones híbridas en tiempo real," *INGE CUC*, vol. 15, no. 2, pp. 11–22, 2019.

[76] C. Riascos, J. Marulanda, and P. Thomson, "Structural control of a grandstand using a semi-active pressurized tuned liquid column damper considering effects of passive crowds," *Structural Control and Health Monitoring*, vol. 26, no. 10, p. e2426, 2019.

[77] A. K. Chopra, *Dynamics of Structures: Theory and Applications to Earthquake Engineering*, Prentice Hall, Hoboken, NJ, USA, 2000.

[78] Z. Chen, J. Liu, and Y. Yu, "Experimental study on interior connections in modular steel buildings," *Engineering Structures*, vol. 147, pp. 625–638, 2017.

[79] C. Chen and J. M. Ricles, "Tracking error-based servohydraulic actuator adaptive compensation for real-time hybrid simulation," *Journal of Structural Engineering*, vol. 136, no. 4, pp. 432–440, 2010.

[80] C. Chen, J. M. Ricles, and T. Guo, "Improved adaptive inverse compensation technique for real-time hybrid simulation," *Journal of Engineering Mechanics*, vol. 138, no. 12, pp. 1432–1446, 2012.

[81] T. Guo, C. Chen, W. Xu, and F. Sanchez, "A frequency response analysis approach for quantitative assessment of actuator tracking for real-time hybrid simulation," *Smart Materials and Structures*, vol. 23, no. 4, Article ID 045042, 2014.

[82] F. Lin, A. Maghareh, S. J. Dyke, and X. Lu, "Experimental implementation of predictive indicators for configuring a real-time hybrid simulation," *Engineering Structures*, vol. 101, pp. 427–438, 2015.